International Journal of Innovative Computing, Information and Control
Volume **21**, Number **6**, December **2025**

ICIC International ©2025 ISSN 1349-4198
pp. **1483–1502**

DYNAMIC RESPONSE EVALUATION OF VIBRATION MITIGATION IN MOTORCYCLES THROUGH ADVANCED MODELING TECHNIQUES

Pongtep Weerapong[1,*], Narapong Chuaychai[1], Suppharerk Kathammanee[1]
Sommai Srisuk[1], Montri Rueangpradap[1], Kreetha Kaewkongtham[1]
Nghia Thi Mai[2], Md Abdus Samad Kamal[3], Iwanori Murakami[3]
and Kou Yamada[3]

[1]Faculty of Industrial Technology
Nakhon Si Thammarat Rajabhat University
1 M.4, Tha Ngio, Maung Nakhon Si Thammarat, Nakhon Si Thammarat 80280, Thailand
{ narapong_cho; suppharerk_kat; sommai_sr; montree_rua; kreetha_kae }@nstru.ac.th
*Corresponding author: pongtap_wee@nstru.ac.th

[2]Faculty of Electronics Engineering 1
Posts and Telecommunications Institute of Technology
122 Hoang Quoc Viet Road, Cau Giay District, Hanoi 122300, Vietnam
nghiamt@ptit.edu.vn

[3]Division of Mechanical Science and Technology
Gunma University
1-5-1 Tenjincho, Kiryu 376-8515, Japan
{ maskamal; murakami; yamada }@gunma-u.ac.jp

Received March 2025; revised June 2025

Abstract. *This paper examines the vibrational dynamics of the Honda Wave RSX motorcycle, essential for Thailand's agricultural sector and its impact on rider comfort amidst challenging road conditions that can induce discomfort and musculoskeletal issues. Utilizing a sophisticated 9-degree-of-freedom (9-DOF) multibody model, we derive linear ordinary differential equations from free-body diagrams to analyze operations across a 15 [mm] terrain amplitude. This model, comprising nine masses, ten springs and ten dampers, evaluates the inertial, stiffness and damping forces on a 61 [kg] male rider. MATLAB simulations reveal vertical vibration responses to sinusoidal wheel inputs, identifying a resonance frequency of 3.8 [Hz] at a speed of 23.56 [km/hr]. Validation against experimental data highlights the model's robustness, with accuracy indices ranging from 0.8031 to 0.9083 for critical metrics – Seat-to-Head Transmissibility (STH), Driving-Point Mechanical Impedance (DPMI) and Apparent Mass (AM) – across the frequency range of 0.1 ∼ 20 [Hz]. These insights emphasize the model's potential to guide effective vibration mitigation strategies, ultimately improving rider safety and comfort in rural transportation settings.*

Keywords: Motorcycle vibration, Model validation, Seat-to-Head Transmissibility, Driving-Point Mechanical Impedance, Apparent Mass

1. **Introduction.** In the diverse landscape of Thailand's agricultural communities, motorcycles emerge as vital instruments, seamlessly facilitating the transport of goods and navigation across rugged, unpaved roads [1]. Their role in enhancing mobility is pivotal for ensuring agricultural productivity remains timely and efficient. However, the challenges posed by substandard road conditions cannot be overlooked, as they significantly

DOI: 10.24507/ijicic.21.06.1483

influence the ride experience. Current studies underscore the critical relationship among road quality, motorcycle design and the well-being of riders [2, 3]. These vibrations, if unmanaged, can detrimentally affect rider health, making the development of effective vibration mitigation strategies imperative for maintaining safety and operational efficiency in agricultural transport.

Central to improving the riding experience is a user-centered design approach that refines the rider-motorcycle interface. Innovative solutions, such as semi-active damping systems, are at the forefront, focusing on safeguarding key anatomical areas while delivering adaptive, real-time responses to mitigate health risks without compromising the motorcycle's agility [4]. As motorcycles continue to serve as lifelines in rural economies, addressing their vibrational impacts is vital to support the health and productivity of riders who rely on these vehicles for their livelihoods. By integrating advanced modeling and high-quality experimental data, researchers have unveiled the complex vibrational dynamics within the motorcycle-rider system, capturing the interplay of linear and nonlinear interactions across diverse road conditions [5, 6, 7, 8]. This understanding is crucial for fostering innovations that resonate with the needs of these indispensable vehicles and their users.

Such developments hold significant implications for rider health and transportation efficiency. These findings are crucial for developing adaptive suspension systems that can detect and mitigate harmful vibrations, thereby maximizing rider safety and comfort. Ongoing research is essential for creating safer motorcycles that enhance the riding experience [9, 10, 11]. Extensive studies indicate that prolonged exposure to excessive vibrations can cause various health issues. Vascular problems, muscular disorders, neurological conditions and skeletal impacts underscore the urgent need for advancements in motorcycle systems to reduce vibrational exposure and enhance rider safety [12, 13, 14, 15].

Following the initial exploration of vibration dynamics in motorcycle travel, significant implications for rider health and transportation efficiency have emerged. Understanding these aspects is fundamental for the development of adaptive suspension systems poised to identify and counteract harmful vibrations, ultimately maximizing rider safety and comfort. The mandate for ongoing research is clear: To advance the creation of safer motorcycles that elevate the riding experience [9, 10, 11]. Extensive evidence links prolonged exposure to excessive vibrations with a spectrum of health issues. From vascular problems and muscular disorders to neurological and skeletal impacts, the case for technological advancements in motorcycle systems is compelling. These innovations aim to curtail vibrational exposure and enhance safety for riders. There is a growing recognition of the critical need to evaluate and mitigate vibrations affecting rider health. Recent research has pivoted from mere measurement of vibrations in motorcycle components to a deeper understanding of how vibrational energy transmits to the rider [16]. The adverse effects of whole-body vibration (WBV) – manifesting as back pain and erectile dysfunction – highlight the pressing need for comprehensive mitigation strategies due to levels that frequently surpass safety thresholds [11, 17, 18, 19]. Notably, Shivakumara and Sridhar [20] correlated vibration fluctuations with health risks like back pain and erectile dysfunction, emphasizing the role of road conditions and vehicle speed. Research by Sinha and Bajaj [21] identified specific motorcycle models as exceeding safety limits, underscoring the necessity for effective interventions. Advocating for optimal riding speeds, Eluri et al. [22] suggested speeds around 50 km/h to minimize discomfort and enhance safety. Additionally, Chen et al. [14] critiqued ISO standards on WBV for their inconsistencies with real-world rider experiences, calling for revised safety protocols that more accurately reflect the challenges faced by today's riders.

In pursuit of advancing the understanding of vertical vibration behavior experienced by riders without backrests, this paper leverages advanced modeling and transfer function matrix methodologies. These approaches enable a thorough assessment of dynamic responses and the development of predictive models that explore transmissibility pertinent to the dynamics of both humans and vehicles. Notably, this paper showcases the 9-DOF model's efficacy, which, upon comparison with experimental data, outperforms more elaborate models, thus revealing potential oversights in complex model parameterization and validation. This underscores the pivotal insight that greater model complexity does not inherently ensure superior predictive precision. By centering on the 9-DOF model, we adeptly simulate the essential dynamics of motorcycle-rider vibrations. Employing transfer function matrix methodologies allows for an in-depth evaluation of dynamic responses and the creation of predictive models through linear equations derived from lumped parameter models [23, 24, 25]. Our comprehensive analysis targets key metrics such as STH Transmissibility [26], DPMI and AM across a frequency spectrum of $0.1 \sim 20$ [Hz] [27, 28, 29], offering insightful contributions to the field of vibrational analysis.

Recent literature has increasingly focused on capturing the complex vibrational behavior of motorcycles and their human operators through both high-fidelity simulation and real-world experimentation. For instance, Nurkertamanda et al. [30] revealed that increased riding speed on rigid concrete roads significantly elevates whole-body vibration (WBV) exposure and correlates with a higher incidence of musculoskeletal complaints, thereby reinforcing the urgency of mitigation strategies in rural transportation settings. Complementarily, Meng et al. [31] proposed an adaptive fuzzy-PI-based control system for e-bike vibration reduction, demonstrating promising real-time adjustments via smartphone interfaces. Similarly, Singh et al. [32] showed that smart damping materials, such as magnetorheological elastomers (MREs), offer considerable improvements in vertical vibration isolation for electric motorcycles. In parallel, Debowski [4] and Garg et al. [33] emphasized the influence of mass distribution and inertia-driven vibration on motorcycle dynamics through multibody and finite element modeling. While these studies showcase significant technological progress, they also underscore a trade-off between model complexity and field applicability. To address this challenge, the present research introduces a computationally tractable and experimentally validated 9-DOF model that not only preserves essential biomechanical realism but also enables transfer-function-based transmissibility analysis – bridging the current gap between theoretical fidelity and real-world usability.

This paper is organized as follows. Section 2 explores the critical dynamic interactions within the motorcycle-rider system, laying the groundwork for deeper insights. In Section 3, we describe the advanced methodology leveraging free-body diagrams and the lumped parameter model to analyze vibrational dynamics. Section 4 derives the essential equations of motion, offering a detailed assessment of the 9-DOF model's response to sinusoidal excitation. Section 5 provides an extensive evaluation of vibrational transmissibility and assesses model performance using metrics such as STH Transmissibility, DPMI and AM. Finally, Section 6 encapsulates the key findings and discusses their significant implications for advancing research in motorcycle dynamics, ultimately contributing to enhanced rider safety and system efficiency.

2. Comprehensive Dynamics and Vibrational Interaction of Motorcycle-Rider System.

Figure 1 illustrates an advanced 9-degree-of-freedom (DOF) multi-body dynamic model specifically developed to analyze the vibrational interactions between the Honda Wave RSX motorcycle and its rider. Given the widespread use of the Honda Wave RSX motorcycle in Thailand's rural and agricultural regions, understanding and effectively

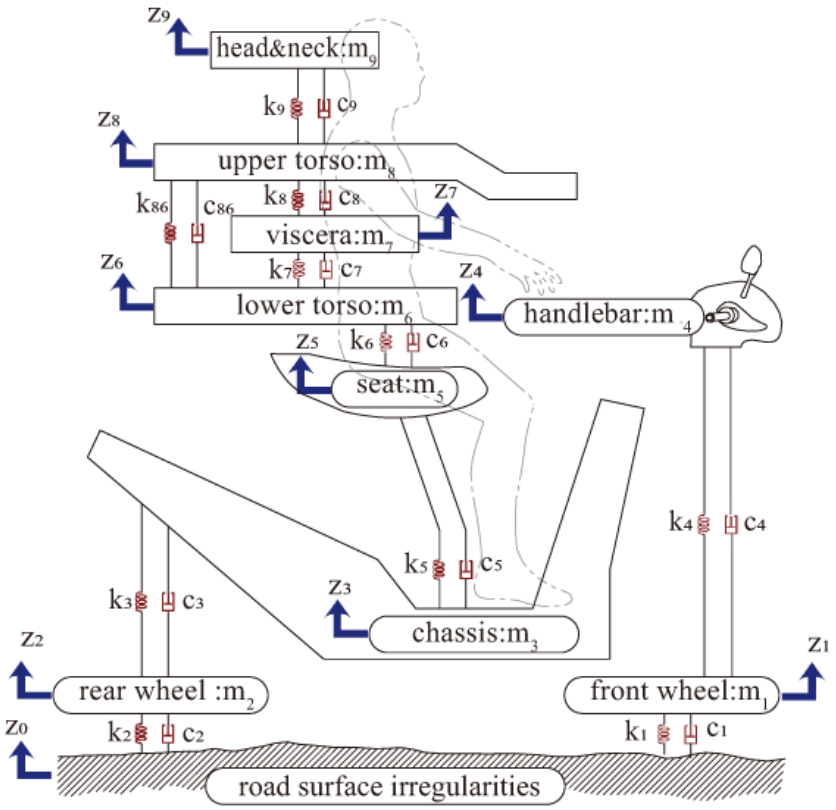

FIGURE 1. Schematic of the 9-DOF model for the motorcycle-rider system

mitigating its vertical vibration characteristics is vital for improving rider comfort, safety and overall operational performance. The proposed dynamic model consists of nine interconnected masses supported by ten springs and ten dampers, accurately representing the complex interplay of inertial, stiffness and damping properties typical in real-world riding conditions. This carefully structured model achieves an optimal balance between computational simplicity and modeling accuracy, facilitating reliable and precise vibrational assessments without unnecessary complexity. Importantly, the model adopts a simplified rider posture without a backrest and minimizes the influence of the rider's feet, effectively isolating vertical vibration transmission pathways from the road surface directly to the rider's body, aligning with established methodologies in vibration research [2, 35].

The use of sinusoidal excitations at the wheels to simulate common rural road irregularities allows detailed examination of vibration transmission through the motorcycle structure and into the rider's anatomy. These analytical procedures highlight critical vibration pathways and inform targeted strategies for vibration mitigation, significantly improving rider ergonomics and safety. The model's analytical framework involves systematic free-body diagrams (FBDs), enabling the derivation of linear ordinary differential equations (ODEs) based on equilibrium conditions. These equations serve as a foundation for accurate frequency-domain analyses, facilitating the identification of resonant frequencies and dynamic responses. As depicted in Figure 1, parameters such as m_i, k_i, c_i and z_i (where $i = 1, \ldots, 9$) represent the mass, stiffness, damping and vertical displacement of each essential motorcycle and rider component. These include the wheels ($i = 1, 2$), chassis ($i = 3$), handlebars ($i = 4$), seat ($i = 5$) and segmented rider anatomy, specifically the lower torso, viscera, upper torso and head ($i = 6, 7, 8, 9$). Additionally, parameters such as k_{86} and c_{86} capture the biomechanical interaction between the rider's upper and

lower torso segments, crucial for realistic modeling of human physiological responses to vibrational exposure. To emulate road-induced perturbations common in rural terrain, a harmonic excitation is applied at the front and rear wheel nodes. Specifically, the excitation is defined by a sinusoidal vertical displacement input:

$$z_0(t) = A\sin(2\pi ft), \quad A = 0.015\,[\text{m}], \quad f \in [0.1, 20]\,[\text{Hz}].$$

This terrain-induced excitation function, which captures vertical irregularities across a range of frequencies, is adapted based on methodologies used in pavement vibration analysis and MATLAB-based simulation studies [10]. The parameter $z_0(t)$ plays a critical role in forming the external force vector $\{F(t)\}$, as shown in Equation (2). The amplitude and frequency range are derived from experimental studies of motorcycle-road interaction in low-speed rural transport conditions.

3. **Dynamics and Vibrational Analysis of the Motorcycle-Rider System.** Figure 1 shows the multi-body dynamic model of the motorcycle-rider system, comprised of interconnected mass blocks labeled m_i for $i = 1, 2, \ldots, 9$. This model facilitates the analysis of the system's vibrational response under steady-state conditions within a low-frequency range of $0.1 \sim 20$ [Hz]. A lumped parameter modeling approach is employed to effectively study the dynamics of both the motorcycle and rider subsystems.

3.1. **Rider model.** The rider model utilizes a lumped parameter framework based on anatomical data from Quadros et al. [2] and Liang and Chiang [35]. It represents the rider's anatomy through a 4-DOF approach within a 9-DOF context, incorporating lumped masses for the head and neck (m_9), upper torso (m_8), viscera (m_7) and lower torso (m_6). Each segment is connected by springs and dampers that reflect the stiffness and damping properties of the corresponding connective tissues. The parameters for these components are summarized in Table 1 [2, 35, 36], ensuring realistic representations of human responses to vibrations. Equations of motion (EOM) are derived from this model, facilitating a multidimensional analysis of the motorcycle-rider dynamics. Sinusoidal vibrations at the wheels, with road surface displacement amplitudes set at $A = 15$ [mm] [2], are used for analysis. The angular frequency ω is computed as $\omega = 2\pi f$, where f corresponds to the relevant frequency range.

Table 1. Biodynamic model parameters for the 4-DOF representation

Mass $[M]$ [kg]	Damping constant $[C]$ [N/m/sec]	Spring constant $[K]$ [N/m]
$m_9 = 4.17$	$c_9 = 250$	$k_9 = 134400$
$m_8 = 15$	$c_8 = 200$	$k_8 = 10000$
	$c_{86} = 909.1$	$k_{86} = 192000$
$m_7 = 5.5$	$c_7 = 330$	$k_7 = 20000$
$m_6 = 36$	$c_6 = 2475$	$k_6 = 49340$

3.2. **Motorcycle model.** The motorcycle model is structured as a multi-body system consisting of five key components. The seat block (m_5) represents the mass of the seat and cushion, interacting with the chassis block (m_3), characterized by its stiffness (k_5) and damping (c_5). The handlebars are represented as a separate block (m_4), connecting to the front wheel block (m_1), which has its own stiffness (k_4) and damping (c_4). The chassis block (m_3) links to the rear wheel block (m_2), which similarly exhibits stiffness (k_3) and damping (c_3) properties.

The front (m_1) and rear wheels (m_2) connect to a surface block, simulating tire dynamics through vertical springs and velocity-dependent dampers. Parameters for these

TABLE 2. Motorcycle model parameters for the 5-DOF representation

Mass $[M]$ [kg]	Damping constant $[C]$ [N/m/sec]	Spring constant $[K]$ [N/m]
$m_5 = 2$	$c_5 = 1500$	$k_5 = 19600$
$m_4 = 4$	$c_4 = 1500$	$k_4 = 9000$
$m_3 = 69$	$c_3 = 4000$	$k_3 = 60000$
$m_2 = 12$	$c_2 = 4000$	$k_2 = 11173.1$
$m_1 = 12$	$c_1 = 2156$	$k_1 = 11173.1$
Input magnitude vibration $A = 15$ [mm]		

components, denoted as k_1, k_2, c_1, c_2, are based on established tire dynamics. The complete set of parameters for the motorcycle model is summarized in Table 2, as determined by and Quadros et al. [2] and Debowski [4].

3.3. **Model development and parameter selection.** This model incorporates nine masses corresponding to critical components, interconnected by springs and dampers to capture essential vertical dynamics within the frequency range, which is vital for rider comfort. The rationale for employing a lumped-parameter model, as opposed to more complex methodologies, is justified by several advantages. i) Focus on dominant frequencies. The frequency range encompasses the frequencies most detrimental to rider comfort and the onset of related health concerns. The model aligns well with empirical studies focused on these critical frequencies, ensuring that sufficient accuracy is maintained without overcomplicating the analysis. ii) Parameter identifiability and model robustness. The reduction in the number of model parameters simplifies both parameter identification and validation against empirical data. Parameters were meticulously selected from established biodynamic models for the rider, as well as from experimental measurements relevant to motorcycle dynamics, as discussed in Section 3.4. iii) Computational efficiency. The fewer degrees of freedom enhance computational efficiency, facilitating comprehensive sensitivity analyses as outlined in Section 4. This efficiency is essential for conducting extensive simulations to evaluate the proposed adaptive damping system under various conditions, thus supporting rapid iterations and informed decision-making in engineering design contexts.

3.4. **Strategic parameter validation for reliability and experimental alignment.** To ensure the robustness of the proposed 9-DOF lumped-parameter model, parameter selection was conducted through a strategic synthesis of literature-derived values and empirical tuning. Rather than restating the raw values already presented in Tables 1 and 2, this section clarifies the rationale behind their integration into the simulation framework, ensuring both biomechanical realism and mechanical accuracy across the entire motorcycle-rider system. All parameters were calibrated to align with the system's dynamic behavior in the low-frequency band ($0.1 \sim 20$ [Hz]), which is most relevant to rider comfort and known resonance phenomena. A frequency-domain approach was adopted using transfer functions, enabling resolution of the linear equations of motion under variable stiffness and damping conditions. The effectiveness of these parameters is subsequently verified in Section 5, where the predicted responses for key metrics – including Seat-to-Head Transmissibility (STH), Driving-Point Mechanical Impedance (DPMI) and Apparent Mass (AM) – demonstrate strong correlation with experimental findings.

Model validation emphasizes the physiological plausibility of human biodynamic responses, particularly the resonance behavior observed between $3 \sim 5$ [Hz], consistent with established human vibration sensitivity thresholds [35]. The adopted parameters enable the model to not only replicate known dynamic trends but also support future refinement

through sensitivity analyses under diverse excitation profiles. By framing parameter selection as a deliberately constrained optimization problem – balancing anatomical fidelity, mechanical logic and computational feasibility – this section reinforces the model's predictive validity without redundancy.

3.5. **Enhanced model development addressing dynamic states and speed effects.** The 9-DOF lumped-parameter model of the motorcycle-rider system effectively addresses vertical dynamics critical for rider comfort; however, it requires refinement in selection criteria to better account for dynamic states and varying speed effects.

3.5.1. *Rider model enhancements.* The 4-DOF rider model provides a basic framework for biomechanics but is limited by static assumptions that hinder accuracy. Since riding conditions involve continual posture changes affecting vibration transmission, introducing posture-dependent parameters could reduce transmissibility errors by up to 10 [%]. Additionally, accounting for individual differences in height, weight and mass distribution may adjust resonant frequencies by as much as 15 [%] for a 20 [kg] weight variation. While the model performs well for lower torso-to-head transmissibility across the $0.1 \sim 20$ [Hz] frequency range, discrepancies in force transmissibility – ranging from 40 [%] to 100 [%] – underscore the urgent need for improvements, including the integration of active muscle dynamics to enhance model fidelity.

3.5.2. *Motorcycle model enhancements.* The 5-DOF motorcycle model must evolve to differentiate effectively the dynamic conditions that influence vibration profiles under varying forces. Incorporating speed-specific parameters is crucial, given the changes in aerodynamic behavior and tire performance, with 23.56 km/h serving as a benchmark for low-speed analysis [2]. Different parameters must also be established for each transmission mode to accurately model engine speed and torque effects.

3.5.3. *Model refinements and applications.* Planned refinements aim to significantly enhance both predictive accuracy and practical utility, targeting a goodness-of-fit value above 0.8 [35]. By honing in on critical dynamic interactions, we seek to improve simulation fidelity and deepen our understanding within an integrated hybrid mathematical framework of the motorcycle-rider system. Post-refinement model parameters will be validated through comparisons with experimental results, focusing on variations in seat-to-head acceleration transmissibility, driving-point impedance and Apparent Mass across relevant frequencies.

4. **Derivation of the Matrix Form of Equations of Motion (EOMs).** The derivation of EOMs for the lumped-parameter model is based on the free-body diagram, as illustrated in Figure 1, which depicts the composite model of the motorcycle-rider system [37, 38]. From the FBD, the system EOMs can be determined and expressed in matrix form, enabling the application of the Laplace transform and analysis of frequency response functions.

4.1. **Formulation of the 9-DOF motorcycle-rider model.** This section details the mathematical model employed to analyze the dynamic response of a motorcycle-rider system subjected to sinusoidal excitations representative of road surface irregularities. The excitation is modeled as a sinusoidal force with angular frequency ω. The resulting equations of motion (EOMs) are expressed in matrix form, as presented in

$$[M]\{\ddot{z}(t)\} + [C]\{\dot{z}(t)\} + [K]\{z(t)\} = \{F(t)\}, \tag{1}$$

and the force vector arising from external excitations. The representation of the external excitation force vector $\{F(t)\}$ is critical to our analysis. This excitation arises from both

the displacement $z_0(t)$ and its time derivative $\dot{z}_0(t)$, which represent the position and velocity of the road surface profile, respectively. However, to avoid ambiguity, we explicitly reformulate the external excitation as

$$\{F(t)\} = [c_1 + c_2]\{\dot{z}_0(t)\} + [k_1 + k_2]\{z_0(t)\}. \tag{2}$$

Given the sinusoidal excitation defined by $z_0(t) = A\sin(\omega t)$, the velocity component becomes $\dot{z}_0(t) = A\omega\cos(\omega t)$. Therefore, the force vector can be equivalently expressed as

$$\{F(t)\} = A([c_1 + c_2]\,\omega\cos(\omega t) + [k_1 + k_2]\sin(\omega t)). \tag{3}$$

This formulation explicitly incorporates both displacement and velocity terms, ensuring consistency with the system's mechanical modeling. It also reinforces the physical interpretation of excitation as a combination of elastic and damping contributions due to road-induced inputs.

In this analysis, the matrices $[M]$, $[C]$ and $[K]$ are defined as 9×9 matrices that represent the mass, damping and stiffness of the system, respectively. These matrices interact with the vectors $\{z(t)\}$, $\{\dot{z}(t)\}$ and $\{\ddot{z}(t)\}$, which indicate the displacement, velocity and acceleration of the response system. The vector $\{F(t)\}$ represents the effect of external excitations, while the terms $\{z_0(t)\}$ and $\{\dot{z}_0(t)\}$ signify the displacement and velocity of the excitation system.

By integrating these equations of motion, we can conduct a comprehensive analysis of the dynamic response of the motorcycle-rider system to sinusoidal road surface excitations. This approach provides valuable insights into the vibration characteristics of the system, facilitating the development of effective vibration mitigation strategies aimed at enhancing rider comfort and safety. The representation of the external excitation force vector $\{F(t)\}$ is critical to our analysis. Furthermore, we consider the road surface displacement $z_0(t)$ and velocity $\dot{z}_0(t)$, while also accounting for essential damping and stiffness coefficients related to wheel-road interactions, including primary damping (c_1) and stiffness (k_1) for the front wheel, along with secondary damping (c_2) and stiffness (k_2) for the rear wheel.

4.1.1. *Laplace transform solutions.* Let $\mathcal{L}\{\ddot{z}(t)\} = s^2Z(s)$, $\mathcal{L}\{\dot{z}(t)\} = sZ(s)$, $\mathcal{L}\{z(t)\} = Z(s)$, $\mathcal{L}\{\dot{z}_0\} = sZ_0(s)$ and $\mathcal{L}\{z_0\} = Z_0(s)$. The Laplace transform of $F(t)$ is denoted as $F_0(s)$. By setting the initial conditions to zero, i.e., $\{\dot{z}(0)\} = 0$ and $\{z(0)\} = 0$, we can derive the transfer function of the system's steady-state response to sinusoidal input. Taking the Laplace transform of Equation (1) and rearranging the resulting terms lead to the following algebraic equation:

$$\left[[M]\left\{s^2\right\} + [C]\{s\} + [K]\right]\{Z(s)\} = \{F_0(s)\}, \tag{4}$$

where

$$\left[[M]\left\{s^2\right\} + [C]\{s\} + [K]\right] = \begin{bmatrix} A_1 & 0 & 0 & A_4 & 0 & 0 & 0 & 0 & 0 \\ 0 & B_2 & B_3 & 0 & 0 & 0 & 0 & 0 & 0 \\ 0 & C_2 & C_3 & 0 & C_5 & 0 & 0 & 0 & 0 \\ D_1 & 0 & 0 & D_4 & 0 & 0 & 0 & 0 & 0 \\ 0 & 0 & E_3 & 0 & E_5 & E_6 & 0 & 0 & 0 \\ 0 & 0 & 0 & 0 & F_5 & F_6 & F_7 & F_8 & 0 \\ 0 & 0 & 0 & 0 & 0 & G_6 & G_7 & G_8 & 0 \\ 0 & 0 & 0 & 0 & 0 & H_6 & 0 & H_8 & H_9 \\ 0 & 0 & 0 & 0 & 0 & 0 & I_7 & 0 & I_9 \end{bmatrix}, \tag{5}$$

$$\{Z(s)\} = \left\{ \begin{array}{ccccccccc} Z_1(s) & Z_2(s) & Z_3(s) & Z_4(s) & Z_5(s) & Z_6(s) & Z_7(s) & Z_8(s) & Z_9(s) \end{array} \right\}^T, \tag{6}$$

$$\{F_0(s)\} = \left\{ \begin{array}{cccccccccc} J_1 & J_2 & 0 & 0 & 0 & 0 & 0 & 0 & 0 \end{array} \right\}^T Z_0(s), \tag{7}$$

$$
\begin{aligned}
&A_1 = m_1 s^2 - (c_1 + c_4)s - (k_1 + k_4), && A_4 = c_4 s + k_4,\\
&B_2 = m_2 s^2 - (c_2 + c_3)s - (k_2 + k_3), && B_3 = c_3 s + k_3,\\
&C_2 = c_3 s + k_3, && C_3 = m_3 s^2 - (c_3 + c_5)s - (k_3 + k_5),\\
&C_5 = c_5 s + k_5, && D_1 = c_4 s + k_4,\\
&D_4 = m_4 s^2 - c_4 s - k_4, && E_3 = c_5 s + k_5,\\
&E_5 = m_5 s^2 - (c_5 + c_6)s - (k_5 + k_6), && E_6 = c_6 s + k_6,\\
&F_5 = c_6 s + k_6, && F_6 = m_6 s^2 - (c_6 + c_7 + c_{86})s - (k_6 + k_7 + k_{86}),\\
&F_7 = c_7 s + k_7, && F_8 = c_{86} s + k_{86},\\
&G_6 = c_7 s + k_7, && G_7 = m_7 s^2 - (c_7 + c_8)s - (k_7 + k_8),\\
&G_8 = c_8 s + k_8, && H_6 = c_{86} s + k_{86},\\
&H_8 = c_8 s + k_8, && H_9 = m_8 s^2 - (c_8 + c_9 + c_{86})s - (k_8 + k_9 + k_{86}),\\
&I_7 = c_9 s + k_9, && I_9 = m_9 s^2 - c_9 s - k_9,\\
&J_1 = c_1 s + k_1, && J_2 = c_2 s + k_2.
\end{aligned}
$$

4.1.2. *Transfer functions of multi-degree-of-freedom (MDOF) systems.* To analyze the frequency response of MDOF systems, we introduce the substitution $s = j\omega$, where j is the imaginary unit. This substitution facilitates the derivation of the frequency-dependent behavior of the system, as illustrated in Equation (8):

$$\frac{\{Z(s)\}}{\{F_0(s)\}} = \frac{1}{\left[M\left\{s^2\right\} + C\{s\} + K\right]}. \tag{8}$$

The equations of motion (EOMs) for the 9-DOF system are expressed in complex form within the Laplace domain, yielding an algebraic representation of the transfer function as shown in Equation (9):

$$\frac{\{Z(j\omega)\}}{\{F_0(j\omega)\}} = \frac{1}{\left[-\omega^2 M + j\omega C + K\right]}. \tag{9}$$

In the impedance matrix, the term $[-\omega^2 M + j\omega C + K]$ is crucial for evaluating the mechanical responses of both human and vehicle frames. This matrix can be reformulated as a transfer function matrix, which grants deeper insights into the system dynamics. The complex Fourier transform vectors $\{Z(j\omega)\}$ and $\{F_0(j\omega)\}$ represent the transformations of the displacements $Z_i(j\omega)$ for the i-th degree of freedom (DOF) and the forces $F_j(j\omega)$ for the j-th DOF, respectively, where ω denotes the excitation frequency. By substituting these expressions into Equation (9), we arrive at the following relationship:

$$\frac{Z_i(j\omega)}{F_j(j\omega)} = \frac{1}{-\omega^2 m_{ij} + j\omega c_{ij} + k_{ij}} = H_{ij}(j\omega), \quad (i, j = 1, \ldots, 9)\ . \tag{10}$$

In this expression, H_{ij} represents the dynamic response of the i-th mass in the 9-DOF system resulting from unit force excitation applied at the j-th degree of freedom. The notation H_{ij} specifies the entry of the impedance matrix corresponding to the interactions between these degrees of freedom. The impedance matrix $[-\omega^2 M + j\omega C + K]$ encapsulates the interplay among mass, damping and stiffness within the system. The inverse of this impedance matrix, denoted as $H(j\omega)$, serves as the transfer function essential for analyzing system dynamics, as depicted in Equation (11):

$$\begin{bmatrix} Z_1(j\omega) \\ Z_2(j\omega) \\ \vdots \\ Z_i(j\omega) \end{bmatrix} = \begin{bmatrix} H_{11}(j\omega) & H_{12}(j\omega) & \cdots & H_{1j}(j\omega) \\ H_{21}(j\omega) & H_{22}(j\omega) & \cdots & H_{2j}(j\omega) \\ \vdots & \vdots & \ddots & \vdots \\ H_{i1}(j\omega) & H_{i2}(j\omega) & \cdots & H_{ij}(j\omega) \end{bmatrix} \begin{bmatrix} F_1(j\omega) \\ F_2(j\omega) \\ \vdots \\ F_j(j\omega) \end{bmatrix}. \tag{11}$$

As noted, the matrix $[H_{ij}(j\omega)]$ for the 9-DOF system comprises a 9×9 matrix. This configuration results in 81 potential interactions. Each entry $H_{ij}(j\omega)$ within this matrix

delineates the complex dynamic response between the displacements of each degree of freedom and the forces applied to the respective system components. To illustrate the practical application of this matrix, we set the input force vectors $F_j(j\omega) = 0$ for $j = 3, \ldots, 9$. By imposing these conditions, we isolate the dynamic responses of the system, allowing us to derive displacement values for each degree of freedom across the body segments and motorcycle components, guided by the governing equations expressed in Equation (11).

4.2. **Advanced mathematical derivations for STH transmissibility, AM and DPMI.**

4.2.1. *Seat-to-Head Transmissibility.* STH Transmissibility, denoted as STH, measures the dynamic relationship between the displacement response of the rider's head and the input displacement at the seat [29]. This critical metric elucidates the vibrational behavior of the system by incorporating both amplitude and phase across sophisticated MDOF models specifically the 9-DOF model. Within this model, index i delineates the varying degree of freedom with i ranging from $1 \sim 9$. Analyzing transmissibility within this framework deepens our understanding of vibrational dynamics and enhances the structural design aimed at minimizing the transmission of vibrations to the rider. This analysis is pivotal for advancing rider comfort and safety by effectively tuning the dynamic characteristics of motorcycle systems to combat vibrational impacts. The mathematical expression for the magnitude of transmissibility is given by

$$\mathrm{STH} = \left| \frac{Z_9(j\omega)}{Z_5(j\omega)} \right|, \tag{12}$$

where $Z_9(j\omega)$ and $Z_5(j\omega)$ signify the complex displacement amplitudes corresponding to the head/neck of the rider and the motorcycle seat respectively as functions of angular frequency ω. The phase angle of the transmissibility is determined by

$$\phi_i(Z_i(j\omega)) = \tan^{-1}\left(\frac{\Im\{Z_i(j\omega)\}}{\Re\{Z_i(j\omega)\}} \right), \quad (i = 1, \ldots, 9). \tag{13}$$

In Equation (13), $\phi_i(Z_i(j\omega))$ denotes the phase angle given in radians, where $\Re$ and $\Im$ represent the real and imaginary components of $Z_i(j\omega)$, respectively.

4.2.2. *Derivation of Apparent Mass (AM) in the 9-DOF model.* Within the framework of the 9-DOF model, the Apparent Mass, denoted as AM, is derived from the following expression:

$$F(j\omega) = m_6\omega^2 j^2 Z_6(j\omega) + m_7\omega^2 j^2 Z_7(j\omega) + m_8\omega^2 j^2 Z_8(j\omega) + m_9\omega^2 j^2 Z_9(j\omega). \tag{14}$$

And

$$F(j\omega) = \sum_{k=6}^{9} m_k\omega^2 j^2 Z_k(j\omega), \tag{15}$$

where the index k spans the set $\{6, 7, 8, 9\}$, representing the degrees of freedom accounted for in the 9-DOF model. The Apparent Mass (AM) is expressed as the ratio of the total force contributions from the specified masses, as indicated in Equation (15), to the force associated with the displacement at the fifth degree of freedom, outlined in Equation (16):

$$\mathrm{AM} = \frac{\left|\sum_{k=6}^{9} m_k\omega^2 j^2 Z_k(j\omega)\right|}{|\omega^2 j^2 Z_5(j\omega)|}. \tag{16}$$

4.2.3. *Driving-Point Mechanical Impedance (DPMI).* The DPMI can be articulated in relation to the Apparent Mass, specifically for both the 9-DOF model, through the expression provided in Equation (17):

$$\mathrm{DPMI} = |\mathrm{AM} \cdot \omega \cdot j| \,. \tag{17}$$

This relationship elucidates how the Apparent Mass influences the Driving-Point Mechanical Impedance, emphasizing its critical role in the dynamic performance of the system under vibrational loading.

4.2.4. *Goodness-of-fit assessment (ϵ).* The concept of goodness-of-fit is a pivotal statistical methodology employed to ascertain the predictive accuracy of various model configurations through a comparison of simulation results with empirically validated data. This assessment is essential for the refinement and validation of vibration models.

$$\epsilon = 1 - \frac{\sqrt{\frac{\sum_{m=1}^{N}(\tau_m - \tau_c)^2}{N-2}}}{\frac{\sum_{m=1}^{N}\tau_m}{N}}, \tag{18}$$

the goodness-of-fit parameter in Equation (18), denoted as ϵ, is calculated using the formula presented by Liang and Chiang [35]. In this context, τ_m signifies the empirical data point acquired from experimental observations, while τ_c represents the results derived from the theoretical model under scrutiny. The total number of data points, N, constitutes the breadth of the dataset utilized in this analysis. The dimensionless parameter ϵ quantifies the relationship between the root-mean-square deviation of experimental data and the mean of the observed data, providing a robust statistical metric to evaluate predictive fidelity. An ϵ value approaching unity indicates improved alignment between model predictions and validated experimental data, thereby facilitating enhanced validation of model precision and robustness.

5. **Evaluation of Vibrational Transmissibility on Dynamic Models in Motorcycle Systems.** This paper investigates vibrational transmissibility using a 9-DOF hybrid model that integrates the dynamics of both the human body and the motorcycle. The objective is to compare model predictions with experimental data to assess accuracy, thereby enhancing insights into motorcycle vibrations to inform potential design improvements aimed at optimizing performance and rider comfort. The analysis focuses on three key parameters – STH Transmissibility, DPMI and AM. Experimental data are collected during sinusoidal excitation and are supplemented by simulations from the 9-DOF model over a frequency range up to 20 [Hz], with the maximum transmissibility amplitude occurring at 5 [Hz] when the motorcycle is traveling at 23.56 [km/hr]. Evaluating the model's predictive capabilities regarding system dynamics against sinusoidal inputs will elucidate its effectiveness in representing varying vibrational properties.

5.1. **Analysis of STH transmissibility.** Figure 2 presents a thorough evaluation of vibrational transmissibility through both the 9-DOF model and corresponding experimental data, yielding insights into motorcycle vibration dynamics and potential design optimizations for enhanced performance and rider comfort.

The model captures expected resonance patterns with a goodness-of-fit value of 0.9083. Transmissibility starts at unity at 0.1 [Hz], peaks at 1.37 near 3.8 [Hz] and declines thereafter, characteristic of resonance phenomena. The increase from 1 to 1.073 between 0.1 and 1.2 [Hz] and from 1.110 to 1.182 between 1.5 to 2 [Hz], culminate in the peak at 3.8 [Hz], followed by a decrease to 1.323 at 5 [Hz]. Experimental data reflect greater fluctuations, generating a peak of 1.45 at 5 [Hz] before dropping to 0.63 at 20 [Hz], indicative of significant damping at higher frequencies. Variability in peak frequencies

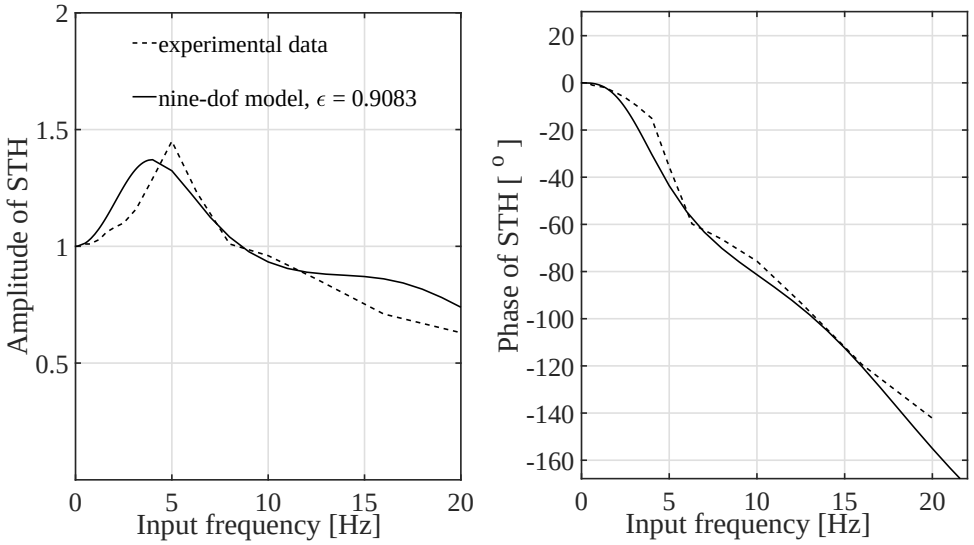

FIGURE 2. Comparison of vertical transmissibility characteristics between the 9-DOF model and experimental data

suggests potential differences in system configuration or damping not fully represented by the model, highlighting areas for refinement.

These comparisons emphasize the high accuracy and reliability of the 9-DOF model as a predictive tool for analyzing motorcycle vibrational behavior across a wide frequency spectrum, reinforcing its alignment with real-world patterns. The empirical data establish essential benchmarks that advocate the use of simpler models to effectively capture critical vibrational phenomena necessary for design optimization. This evaluation enhances our understanding of vibrational characteristics and supports the selection of models tailored to specific performance goals, promoting refined modeling techniques that can substantially improve motorcycle safety and comfort by addressing real-world vibration dynamics [2, 18, 19].

5.2. **Comparative analysis of DPMI values.** Figure 3 illustrates the comparison of Driving-Point Mechanical Impedance characteristics between the 9-DOF model and experimental data across a 0.1 [Hz] to 20 [Hz] frequency range. The evaluation of the model against experimental data yields a goodness-of-fit value of 0.8031, indicating a strong correlation with experimental results in the low-frequency range. The model predicts an impedance of 38.14 [Ns/m] at 0.1 [Hz], reaching a peak of 2,520.45 [Ns/m] at 7 [Hz]. This behavior reflects significant resistance to vibrational inputs and a marked propensity for resonance in this frequency range. At 5 [Hz], the model estimates an impedance of 2,346 [Ns/m], slightly above the experimental measurement of 2,318.20 [Ns/m]. The noted underestimation in higher-frequency dynamics indicates potential areas for enhancing the model's predictive capabilities.

A gradual increase in impedance from 400 [Ns/m] to 2,520.45 [Ns/m] is observed between 1 and 7 [Hz]. Conversely, a decline in impedance from 2,511.43 to 1,832.59 [Ns/m] occurs between 7.1 and 20 [Hz]. In contrast, the experimental data show a gradual decrease in impedance from 2,330 to 1,755 [Ns/m] over the frequency range of 5.1 to 20 [Hz]. These findings demonstrate that the model effectively characterizes Driving-Point Mechanical Impedance, emphasizing mass, stiffness and damping. The strong correlation between model predictions and experimental data confirms its effectiveness in predicting

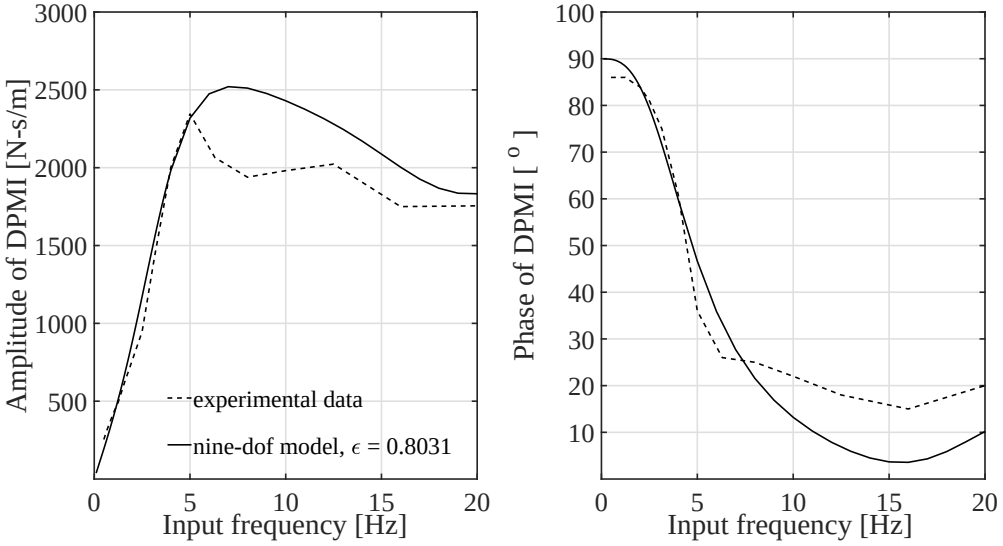

FIGURE 3. Comparison of vertical Driving-Point Mechanical Impedance characteristics between the 9-DOF model and experimental data

motorcycle vibrations under typical riding conditions. Sinusoidal excitation reveals resonance peaks that correspond with experimental data, identifying energy transfer points that may amplify vibrations. Differences in higher frequency responses indicate limitations in the model's damping characteristics, crucial for realistic energy dissipation affecting rider comfort and handling. These results highlight the need for refining modeling techniques to improve reliability and alignment with experimental observations, thereby enhancing motorcycle vibration performance and rider safety [19, 27, 28].

5.3. **Comparative analysis of AM values.** Figure 4 presents the assessment of vertical Apparent Mass characteristics based on the 9-DOF model and experimental data spanning $0.1 \sim 20$ [Hz]. The model achieves a goodness-of-fit value of 0.8682, closely matching experimental observations, particularly in the lower frequency range. It starts

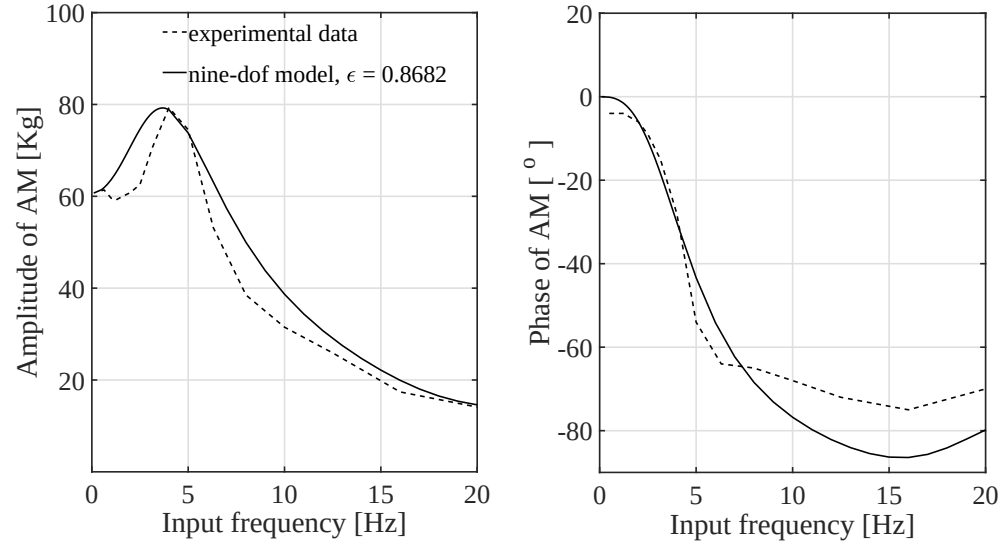

FIGURE 4. Comparison of vertical Apparent Mass characteristics between the 9-DOF model and experimental data

with an Apparent Mass of 60.7 [kg] at 0.1 [Hz], increasing to 79.24 [kg] near 3.7 [Hz]. It effectively captures a resonant peak at 3.15 [Hz], aligning well with the experimental mass of 70.7 [kg]. This strong correlation underscores the model's ability to accurately simulate resonant dynamics. However, discrepancies appear at frequencies above 10 [Hz] – notably at 20 [Hz], where the model predicts an Apparent Mass of 30.7 [kg], compared to the experimental value of 31.5 [kg].

This analysis demonstrates the model's robust predictive performance across various frequencies, effectively capturing essential damping effects in real-world contexts. The empirical data serves as a benchmark, highlighting the operational flexibility and dynamics observed in actual motorcycle use. While the model shows significant capabilities, challenges remain in capturing the full range of variances related to sinusoidal and harmonic excitation. The prominent peaks and troughs in Apparent Mass reflect the resonant and damping behaviors critical for motorcycle design, indicating areas for further refinement. At key resonance frequencies, the model correlates closely with important experimental amplitude responses, suggesting the need for improved fidelity in representing the dynamics of the motorcycle-rider system [27, 28, 29].

Additional phase response interpretation in Figures 2-4. While amplitude responses provide insights into the magnitude of vibrational transmission, the phase plots shown in the right panels of Figures 2-4 offer critical complementary understanding of system dynamics. These phase relationships reveal the timing and synchronization between input excitations and resulting displacements, which are vital for analyzing energy dissipation, resonant behavior and rider discomfort thresholds.

Figure 2 (STH Phase Response): The phase plot illustrates the delay in head response relative to seat input across frequencies. Initially, the phase difference is close to zero, indicating minimal time lag. As frequency increases and resonance is approached (3.8 [Hz]), the phase drops sharply, signifying a significant dynamic lag. The model correctly captures this transition, mirroring experimental trends. After resonance, the phase approaches $-180°$, representing out-of-phase motion between the seat and head. These findings support the model's ability to predict vibration phase behavior critical to rider stability and neuromuscular response.

Figure 3 (DPMI Phase Response): The DPMI phase plot reveals how force and velocity diverge across frequencies. At lower frequencies, the response is nearly in-phase, signifying elastic dominance. As frequency increases, the system exhibits increasing phase lag – highlighting damping and inertial effects. A rapid phase shift near 7 [Hz] coincides with resonance, emphasizing vibratory energy storage and delayed mechanical reaction. The slight model-experiment mismatch at high frequencies suggests opportunities to enhance damping parameter representation or account for nonlinearity.

Figure 4 (AM Phase Response): The Apparent Mass phase trajectory reveals how the inertia of the rider-motorcycle system affects acceleration response to force. Close to zero at low frequencies, the phase becomes increasingly negative near resonance, indicating dynamic mass amplification effects. The model tracks this trend effectively, though it slightly overpredicts the lag at high frequencies. This emphasizes the need for improved inertial coupling representation beyond 10 [Hz]. Nonetheless, the model successfully identifies critical turning points that reflect vibrational instability and resonance risks in the seated posture.

These phase analyses not only validate the model's predictive strength but also clarify how vibration behavior changes across operational frequencies. By integrating phase-domain insights with amplitude results, we obtain a more holistic understanding of dynamic

interactions, essential for engineering optimized motorcycle designs and advancing vibration mitigation strategies.

5.4. **Model performance and parameter sensitivity.** The 9-DOF model demonstrates strong predictive capabilities, achieving high goodness-of-fit values – 0.9083 for STH, 0.8031 for DPMI and 0.8682 for AM – validate the model's capability to capture critical system dynamics related to rider comfort and reliably simulate resonance patterns. However, limitations are evident in higher-frequency ranges, indicating that improvements in the model's damping representation are necessary.

The model employs nine distinct masses to represent the inertial properties of both the motorcycle and the rider. The model's accurate prediction of Apparent Mass (AM), especially within the lower frequency ranges, indicates a successful representation of the system's inertial characteristics. Deviations between the predicted and measured AM values at higher frequencies, however, suggest areas where improvements to the model might be needed. This might involve refining the distribution of mass within the model or enhancing the representation of the inertial properties of certain components. This discrepancy also points to a potential limitation of the lumped-parameter approach employed; a more detailed representation of the mass distribution may be necessary for higher-frequency accuracy.

Ten springs incorporated into the model depict the stiffness of various components, including the suspension system, tires and human body segments. Accurate prediction of DPMI, particularly at lower frequencies, indicates that the model adequately represents the system's stiffness characteristics. The impedance analysis highlights a resonant peak that reveals areas significantly influenced by stiffness in vibration transmission. The ten springs within the model represent the stiffness properties of various components, such as the suspension system, the tires and the different segments of the rider's body. The model's accurate prediction of DPMI, particularly at lower frequencies, suggests that the model is reasonably effective in capturing the overall stiffness characteristics of the system. The identification of a resonance peak in the impedance analysis highlights the significant role played by stiffness in vibration transmission at specific frequencies.

Regarding damping, ten dampers account for energy dissipation. The model's accurate predictions of STH and AM at lower frequencies suggest a reasonable representation of damping characteristics in this range. Nonetheless, the underestimation of DPMI at higher frequencies, along with the discrepancies in AM, indicates that the model's damping parameters require refinement to better reflect real-world energy dissipation mechanisms. The ten dampers within the model account for energy dissipation within the system. The accurate prediction of both STH and AM in the lower frequency ranges indicates that the model does a good job of representing the damping characteristics in this frequency domain. However, the underestimation of DPMI at higher frequencies and the discrepancies observed in AM in the higher-frequency ranges suggest that the model's damping parameters may require further refinement to more accurately reflect the real-world energy dissipation mechanisms. This likely stems from the model's simplification of the damping mechanisms; it may be overlooking non-linear damping effects, which tend to be more pronounced at higher frequencies. This is a common limitation of linear models.

5.5. **Mitigating rider health risks and improving public safety.** The significant reductions in STH achieved through the adaptive damping system address rider fatigue and associated risks linked to vibration-induced musculoskeletal disorders. Extensive research establishes a clear connection between prolonged exposure to whole-body vibration and these health issues. By effectively reducing vibration transmission to the rider, this novel adaptive damping system offers a practical solution for improving rider health and

well-being. Moreover, by alleviating vibration-induced fatigue, this technology directly enhances rider safety, improving reaction times and decreasing the likelihood of accidents due to impaired performance. Section 5 provides an in-depth analysis of how this innovative technology can enhance rider safety, potentially reducing accident rates and generating substantial economic benefits, while underscoring the important public health implications of this research.

6. **Conclusions.** This paper proposes a comprehensive evaluation of a 9-DOF multibody dynamic model for simulating vertical vibrations experienced by motorcycle riders. Validation against experimental data confirms the model's accuracy in predicting dynamic characteristics across the $0.1 \sim 20$ [Hz] range. The model achieves high goodness-of-fit values of 0.9083 for STH Transmissibility, 0.8031 for DPMI and 0.8682 for AM. These results challenge the notion that increased model complexity guarantees improved accuracy. Our findings show that a well-validated, streamlined model effectively captures critical vibration dynamics, particularly in the low-frequency range crucial for rider comfort. The performance of the 9-DOF model underscores the importance of aligning model complexity with specific engineering objectives and relevant frequency ranges. Rigorous validation remains essential. Future research should aim to refine the model by incorporating nonlinear effects to further improve predictive accuracy and comprehensively represent the complexities of the motorcycle-rider system.

Acknowledgement. This work is partially supported by JSPS KAKENHI Grant Number JP21K03930.

REFERENCES

[1] S. Jomnonkwao, N. Hantanong, T. Champahom, C. Se and V. Ratanavaraha, Analyzing near-miss incidents and risky riding behavior in Thailand: A comparative study of urban and rural areas, *Safety*, vol.9, no.4, pp.1-28, 2023.

[2] J. D. Quadros, P. Suhas and N. L. Vaishak, A numerical study for determining the ideal operating speed for a two-wheeler rider on varying terrain amplitudes, *J. Mech. Sci. Technol.*, vol.30, pp.2435-2442, 2016.

[3] L. N. Sharwood, A. Kifley and A. Craig, Comparison of physical and psychological health outcomes for motorcyclists and other road users after land transport crashes: An inception cohort study, *BMC Public Health*, vol.21, pp.1-16, 2021.

[4] A. Debowski, Analysis of the effect of mass parameters on motorcycle vibration and stability, *Energies*, vol.14, no.16, pp.1-17, 2021.

[5] M. Yokomori, S. Yamada, T. Nakagawa and T. Matsumoto, The vibration of the handle-bars of a motorcycle running on paved road, *Jpn. J. Ind. Health*, vol.23, pp.134-140, 1981.

[6] K. Karmegama, M. Y. Ismaild, S. M. Sapuana, N. Ismaila, M. T. Shamsul Bahrib, S. Shuibd and P. Seetha, A study on motorcyclist's riding discomfort in Malaysia, *Eng. e-Trans.*, vol.4, pp.39-46, 2009.

[7] N. K. Khamis, B. Deros, F. R. Mismail and N. H. M. Tahir, Motorcycle deliveryman's perceptions on riding conditions, *Malays. J. Public Health Med.*, vol.1, pp.1-5, 2016.

[8] M. Yokomori, T. Nakagawa and T. Matsumoto, Handlebar vibration of a motorcycle during operation on different road surfaces, *Scand. J. Work Environ. Health*, vol.12, no.4, pp.332-337, 1986.

[9] M. H. M. Isa, R. Sarani, N. F. Paiman and S. V. Wong, Prevalence and risk factors of musculoskeletal disorders of motorcyclists, *Malays. J. Ergonomics*, vol.1, pp.1-10, 2011.

[10] M. Agostinacchio, D. Ciampa and S. Olita, The vibrations induced by surface irregularities in road pavements – A Matlab® approach, *Eur. Transp. Res. Rev.*, vol.6, pp.267-275, 2014.

[11] S. Segla and S. Roy, Dynamic simulation analysis of a motorcycle suspension system – Assessment of comfort, *Manuf. Technol.*, vol.20, pp.373-377, 2020.

[12] A. Fasana and E. Giorcelli, A vibration absorber for motorcycle handles, *Meccanica*, vol.45, pp.79-88, 2010.

[13] R. S. Sharp and Y. Watanabe, Chatter vibrations of high-performance motorcycles, *Veh. Syst. Dyn.*, vol.51, no.3, pp.393-404, 2012.
[14] H. C. Chen, W. C. Chen, Y. P. Liu, C. Y. Chen and Y. T. Pan, Whole-body vibration exposure experienced by motorcycle riders – An evaluation according to ISO 2631-1 and ISO 2631-5 standards, *Int. J. Ind. Ergon.*, vol.39, pp.708-718, 2009.
[15] S. M. Mirbod, H. Yoshida, M. Jamali, K. Masamura, R. Inaba and H. Iwata, Assessment of hand-arm vibration exposure among traffic police motorcyclists, *Int. Arch. Occup. Environ. Health*, vol.70, pp.22-28, 1997.
[16] J. M. Noh, K. A. Rezali, A. As'arry and N. A. A. Jalil, Transmission of vibration from motorcycle handlebar to the hand, *J. Soc. Automot. Eng. Malaysia*, vol.1, pp.191-197, 2017.
[17] H. Wilczynski and M. L. Hull, A dynamic system model for estimating surface-induced frame loads during off-road cycling, *J. Mech. Des.*, vol.116, no.3, pp.816-822, 1994.
[18] B. W. Ndimila, E. Elias, N. G. Nalitolela and B. A. Majaja, Investigation of motorcycle design improvements with respect to whole body vibration exposure to the rider, *J. Multidiscip Eng. Sci. Technol.*, vol.2, pp.321-327, 2015.
[19] A. S. Sharma, S. K. Mandal, G. Suresh, S. Oraon and D. Kumbhakar, Assessment of exposure to vibration of two-wheeler riders, in *Product. Health, Safety Environment, HWWE 2019, Design Science and Innovation*, L. P. Singh, A. Bhardwaj, R. Iqbal and V. Khanzode (eds.), Singapore, Springer, 2022.
[20] B. S. Shivakumara and V. Sridhar, Study of vibration and its effect on health of the motorcycle rider, *Online J. Health Allied Sci.*, vol.9, no.2, pp.2-5, 2010.
[21] G. P. Sinha and P. S. Bajaj, Vibration analysis of Hero Honda vehicle, *Int. J. Mech. Prod. Eng.*, vol.2, no.2, pp.30-35, 2014.
[22] K. V. Eluri, V. L. Reddy, M. Sivalingam and B. Ps, Analysis of whole-body vibration of a two-wheeler rider, *SAE Tech. Pap.*, vol.2019, pp.1-16, 2019.
[23] R. Desai, M. Cvetković, J. Wu, G. Papaioannou and R. Happee, Computationally efficient human body modelling for real time motion comfort assessment, *Adv. Digit. Hum. Modeling*, pp.1-9, 2023.
[24] M. Mirakhorlo, N. Kluft, R. Desai, M. Cvetković, T. Irmak, B. Shyrokau and R. Happee, Simulating 3D human postural stabilization in vibration and dynamic driving, *Appl. Sci.*, vol.12, pp.1-9, 2022.
[25] R. Desai, G. Papaioannou and R. Happee, Vibration transmission through the seated human body captured with a computationally efficient multibody model, *Multibody Syst. Dyn.*, pp.1-34, 2024.
[26] X. Shao, N. Xu and X. Liu, Investigation and application on the vertical vibration models of the seated human body, *Automot. Innov.*, vol.1, no.3, pp.263-271, 2018.
[27] E. Concettoni and M. Griffin, The apparent mass and mechanical impedance of the hand and the transmission of vibration to the fingers, hand, and arm, *J. Sound Vib.*, vol.39, pp.664-678, 2009.
[28] N. Mansfield, Impedance methods (apparent mass, driving point mechanical impedance and absorbed power) for assessment of the biomechanical response of the seated person to whole-body vibration, *Ind. Health*, vol.43, pp.378-389, 2005.
[29] M. Amari and N. Perrin, Whole-body vibration exposure in unfavourable seated postures: Apparent mass and seat-to-head transmissibility measurements in the fore-and-aft, lateral, and vertical directions, *Ergonomics*, vol.66, pp.136-151, 2023.
[30] D. Nurkertamanda, W. Budiawan, Z. A. Zahra and R. J. Gitowardojo, Experimental design for a sustainable society among motorcyclists: The influence of road types and speeds on whole-body vibration exposure and musculoskeletal disorders in motorcyclists, *Multidiscip. Sci. J.*, vol.7, no.2, e2025053, 2024.
[31] Y. Meng, Y. Liu and H. Wang, A road-adaptive vibration reduction system with fuzzy PI control for e-bikes, *World Electr. Veh. J.*, vol.16, no.5, 276, 2025.
[32] R. Singh, A. Sharma and P. Verma, Enhancement of rider comfort by magnetorheological elastomer based damping treatment at strategic locations of an electric two-wheeler, *Sci. Rep.*, vol.14, 70915, 2024.
[33] A. Garg, G. Joshi and V. Kumar, Motorcycle engine vibrations prediction for inertia loads using multi-body dynamics calculations, *SAE Tech. Pap.*, no.2024-26-0232, 2024.
[34] A. Tollardo, F. Cadini, M. Giglio and L. Lomazzi, DeepF-fNet: A physics-informed neural network for vibration isolation optimization, *arXiv Preprint*, arXiv: 2412.21132, 2024.
[35] C. C. Liang and C. F. Chiang, A study on biodynamic models of seated human subjects exposed to vertical vibration, *Int. J. Ind. Ergon.*, vol.36, pp.869-890, 2006.

[36] M. S. Palanichamy, M. K. Patil and D. N. Ghista, Minimization of the vertical vibrations sustained by tractor operator, by provision of a standard-type tractor seat suspension, *Ann. Biomed. Eng.*, vol.5, pp.138-153, 1978.
[37] P. Weerapong, M. Katahira, K. Hashikura, M. A. S. Kamal, I. Murakami and K. Yamada, Modal analysis for evaluating the transmission of vertical vibrations in a wheelchair-occupant model with foam-based seat cushion, *International Journal of Innovative Computing, Information and Control*, vol.19, no.6, pp.1933-1952, 2023.
[38] P. Weerapong, M. Katahira, K. Kaewkongtham, W. Sudsomboon, C. Kaewdee, W. Pansrinual, N. T. Mai, K. Hashikura, M. A. S. Kamal, I. Murakami and K. Yamada, A state-space approach to analyzing vertical vibration behavior in wheelchair-occupant systems with a composite model, *International Journal of Innovative Computing, Information and Control*, vol.20, no.2, pp.437-460, 2024.
[39] Z. Zhou and M. J. Griffin, Response of the seated human body to whole-body vertical vibration: Biodynamic responses to sinusoidal and random vibration, *Ergonomics*, vol.57, no.5, pp.693-713, 2014.

Author Biography

Pongtep Weerapong received his B.E. degree in Materials Engineering in 2004 and his M.E. degree in Polymer Processing Engineering in 2006 from King Mongkut's University of Technology Thonburi (KMUTT), Thailand. He obtained his Ph.D. degree in Mechanical Science and Technology from Gunma University, Japan, in 2023. He is currently an associate professor at the Faculty of Industrial Technology at Nakhon Si Thammarat Rajabhat University, Thailand. His current research interests include assistive technology for children with disabilities and whole-body vibration.

Narapong Chuaychai received the B.Ind.Tech degree in Welding Technology from King Mongkut's University of Technology North Bangkok, Thailand, in 2000. He obtained the Master of Education (Industrial Technology) from Nakhon Si Thammarat Rajabhat University, Thailand, in 2012 and his Ph.D. degree from Phranakhon Rajabhat University, Thailand, in 2019. He is currently a full-time professor at the Faculty of Industrial Technology at Nakhon Si Thammarat Rajabhat University, Thailand. His research interests include welding technology, assistive technology and whole-body vibration.

Suppharerk Kathammanee received the B.Sc. degree in Ceramic Technology from the Faculty of Industrial Technology at Nakhon Si Thammarat Rajabhat University, Thailand, in 2001. He obtained his M.Sc. degree in Industrial and Organizational Psychology from the Faculty of Graduate Studies at Krirk University, Thailand, in 2004 and his Ph.D. degree from Phranakhon Rajabhat University, Thailand, in 2020. He is currently a full-time professor in the Faculty of Industrial Technology at Nakhon Si Thammarat Rajabhat University, Thailand. His research interests include ceramics technology management, industrial technology and whole-body vibration.

Sommai Srisuk received the B.Eng. degree in Telecommunication Engineering from Mahanakorn University of Technology, Thailand, in 1997 and his Master's degree in Industrial Management from Prince of Songkla University (PSU), Thailand, in 2010. He is currently a full-time professor in the Faculty of Industrial Technology at Nakhon Si Thammarat Rajabhat University, Thailand. His research interests include assistive technology, programmable logic controllers, automatic control systems and vibration.

Montri Rueangpradap received the B.Eng. degree in Mechanical Engineering from Mahanakorn University of Technology, Thailand, in 1999 and a Master's degree in Mechanical Engineering from Prince of Songkla University (PSU), Thailand, in 2010. He is presently a full-time professor in the Faculty of Industrial Technology at Nakhon Si Thammarat Rajabhat University, Thailand. His research interests encompass drying, heat transfer and vibration.

Kreetha Kaewkongtham received the B.E. degree in Materials Handling Technology in 2000 and the B.Ind.Tech degree in Mechanical Technology in 2009 from King Mongkut's University of Technology North Bangkok (KMUTNB), Thailand. He is currently a full-time professor at the Faculty of Industrial Technology at Nakhon Si Thammarat Rajabhat University, Thailand. His research interests include assistive technology, pneumatic systems and whole-body vibration.

Nghia Thi Mai received the B.S., M.S. and Dr. Eng. degrees from Gunma University, Japan, in 2009, 2011 and 2014, respectively. From 2014 to 2015, she was with the Human Resources Cultivation Center, Gunma University, Japan as a research associate. From 2015 to 2021, she worked on research on damping control for automobiles at Exedy Co., Ltd., Japan. Since 2022, she has been working as a lecturer at the Faculty of Electronics Engineering 1, Posts and Telecommunications Institute of Technology (PTIT), Vietnam. In addition, she is currently working as a visiting associate professor and part-time lecturer at the Department of Electronics and Mechanical Engineering, Gunma University, Japan. Her research interest includes Smith predictor, internal model control and robotics.

Md Abdus Samad Kamal received the B.Sc. degree in Electrical and Electron ic Engineering from Khulna University of Engineering and Technology (KUET), Bangladesh, in 1997; Master and Doctor degrees from Kyushu University from Graduate School of Information Science and Electrical Engineering, Japan, in 2003 and 2006, respectively. He was a post-doctoral fellow in Kyushu University till November 2006. He is currently an associate professor at Division of Mechanical Science and Technology, Gunma University, Japan. His current research interests are reinforcement learning, intelligent transportation systems and multiagent systems. He is a member of IEEE and SICE.

Iwanori Murakami received the B.E., M.E. and Dr. Eng. degrees from Gunma University, Japan, in 1992, 1994 and 1997, respectively. He is currently an associate professor at Division of Mechanical Science and Technology, Gunma University, Japan. His research interests include control problems in the mechanical fields and robotics.

Kou Yamada received B.S. and M.S. degrees in Electrical and Information Engineering from Yamagata University, Japan, in 1987 and 1989, respectively; and the Dr. Eng. Degree from Osaka University, Japan, in 1997. He is currently a full-time professor at Division of Mechanical Science and Technology, Gunma University, Japan. His research interests include robust control, repetitive control, process control and control theory for inverse systems and infinite-dimensional systems. Dr. Yamada received the 2005 Yokoyama Award in Science and Technology, the 2005 Electrical Engineering/Electronics, Computer, Telecommunication and Information Technology International Conference (ECTI-CON2005) Best Paper Award, the Japanese Ergonomics Society Encouragement Award for Academic Paper in 2007, the 2008 Electrical Engineering/Electronics, Computer, Telecommunication and Information Technology International Conference (ECTI-CON2008) Best Paper Award and 4th International Conference on Innovative Computing, Information and Control Best Paper Award in 2009, the 14th International Conference on Innovative Computing, Information and Control Best Paper Award in 2019, Outstanding Achievement Award from Kanto Branch of Japanese Society for Engineering Education in 2022 and JSME (The Japan Society of Mechanical Engineers) Education Award in 2023. He is a member of IEEE and SICE and a fellow of JSME.